# Assessment of Urban Heat Island Patterns in Bangkok Metropolitan Area Using Time-Series of LANDSAT Thermal Infrared Data

**Warisara Sanecharoen[1], Kanchana Nakhapakorn[1*], Aeumphorn Mutchimwong[1], Supet Jirakajohnkool[2], and Rattapon Onchang[3]**

*[1]Faculty of Environment and Resource Studies, Mahidol University, Nakhon Pathom 73170, Thailand*
*[2]Faculty of Science and Technology, Thammasat University, Pathum Thani 12120, Thailand*
*[3]Faculty of Science, Silpakorn University, Nakhon Pathom 73000, Thailand*

**ARTICLE INFO**

Received: 19 Feb 2019
Received in revised:
6 Jun 2019
Accepted: 14 Jun 2019
Published online:
26 Aug 2019
DOI: 10.32526/ennrj.17.4.2019.34

**Keywords:**
Land surface temperature/
Surface urban heat island/
LANDSAT TM image/ NDVI

**[*]Corresponding author:**
E-mail:
kanchana.nak@mahidol.ac.th

**ABSTRACT**

Bangkok is a rapidly expanding city with existing natural areas being replaced by developed areas creating an urban heat island (UHI) phenomenon in the city. LANDSAT imagery, near-infrared wavelength data, and time series information were used to study and to monitor the phenomenon of surface urban heat island (SUHI) in Bangkok. The variation of land surface temperature (LST) and the urban heat island intensity (UHII) phenomenon during 2008-2014 were investigated and the relationship between the UHII phenomenon and urban sprawl in Bangkok was studied. Using the UHII, we compared nine LST images of the investigated areas defined as inner, urban fringe and suburb zones. The UHI in Bangkok in the winter (dry) is higher than in the summer. Satellite imageries were used to classify the land use types as open spaces with high-rise buildings, very high density of buildings and high-rise buildings. Low vegetation index was found in urban fringe areas and inner city area with high surface temperature. The vegetation index value is high in areas of agricultural land, and low density building, it appears in suburb areas with low surface temperature. The results indicate that NDVI and High-rise building zones influence LST distribution and UHII phenomenon.

## 1. INTRODUCTION

Currently, the expansion of urban space transforms the existing natural areas into areas covered by built-up areas such as buildings, roads, and sidewalks, most of which are impervious materials. It has the properties of low solar energy but it absorbs energy from the sun. This causes heat accumulation in the urban area. Consequently, the temperature in the urban area is higher than in the suburbs or rural areas, creating an effect called an urban heat island (UHI) (Voogt and Oke, 2003; Grimm et al., 2008; U.S. EPA, 2014). The urban heat island phenomenon has an impact on many urban environments, such as increasing the demand for cooling energy. The increased use of energy also leads to emissions of air pollution and greenhouse gases. It also affects the quality of life and health of the urban population and causes irritation of the respiratory tract, physical discomfort and fatigue Including illness or death due to heat (Grimm et al., 2008; U.S. EPA, 2014).

Monitoring of urban heat island phenomena can be done in two ways (Jiang et al., 2006; U.S. EPA, 2014). The first method is an air quality monitoring station or mobile air quality monitoring. However, this method is limited because the number of stations may not be sufficient to cover the study area. Especially in cases where the study area is large, the spatial information is not detailed (Streutker, 2003; Meng and Liu, 2013). Another way is using remote sensing technology including data from thermal infrared band to study land surface temperature (LST) of the desired area. This approach has the advantage of being effective in displaying conditions continuously and collecting spatial data throughout the study area. It can remotely monitor the temperature changes in the same area quickly and provide acceptable results at an acceptable level. Originally, most studies of LST to describe UHI phenomena were based on thermal infrared bands from the AVHRR (Advanced Very High Resolution Radiometer) and MODIS (Moderate Resolution Imaging Spectroradiometer). This data is still collected up to this date (Hung et al., 2006; Imhoff et al., 2010; Pongrácz et al., 2010; Keramitsoglou et al., 2011; Zhou et al., 2014). However, the thermal

infrared bands from AVHRR and MODIS have a low resolution of about 1 km, which is suitable for studying and mapping regional LST, but is not suitable for studying the relationship between LST and physical-biological features in the city (Streutker, 2002; Weng et al., 2014; Tongliga et al., 2016).

Hence, the higher resolution thermal infrared bands, e.g., LANDSAT TM/ETM+ (resolution of 120 and 60 m, respectively) as well as ATLAS (Advanced Thermal and Land Applications Sensor) (resolution of 2 m resolution), have been used to study the variation of LST in urban areas and their relation to land use and land cover (Nichol, 1996; Lo et al., 1997; Qin et al., 2001; Xu and Chen, 2004; Chen et al., 2006; Yuan and Bauer, 2007; Weng et al., 2007; Li et al., 2012; Meng and Liu, 2013; Balçik, 2014; Manjula et al., 2017). The data from the LANDSAT satellite is highly detailed, with the potential to monitor LST and UHI phenomena (Weng et al., 2014; Zhang et al., 2017). Until present, there have been many researches on the LST and UHI patterns, especially in megacities. However, those studies have often used a limited amount of satellite data in the study. Hung et al. (2006) and Li et al. (2012) proposed that the time-series satellites data used to study LST will result in finer and better results. Then, this study focuses on utilizing time-series LANDSAT TM/TIRS, thermal infrared bands to study and monitor the phenomenon of UHI in the Bangkok Metropolitan Area (BMA). It aims at studying variation of LST and UHI intensity (UHII) in BMA during the years from 2008-2014; and studying the relationship between the UHII, land use and land cover, and the expansion of urban areas in BMA. Bangkok has continuously expanded its urban area from past to present. While the study on BMA heat island phenomenon is relatively low, the results of the past research showed that Bangkok is experiencing the phenomenon of heat island, especially in urban areas and main roads with high and dense buildings, and less vegetation (Komonveeraket, 1998; Teanmanee, 2002; Chayapong, 2010). Hung et al. (2006) found that in February 2002, the central area of BMA had a higher LST than the large urban parks and suburbs of around 5-6 $^{o}$C.

## 2. METHODOLOGY

### 2.1 Data and quality control tests

In this study, 46 (44) records of monthly rainfall (mean surface air temperature) data routinely measured at the surface weather stations of the Thai Meteorological Department (TMD) distributed across Thailand were used. The data were first selected on the basis of record length being available from 1961 to 2016 and completeness with missing data less than 1%. All selected data were subjected to a further statistical quality control (QC) algorithm. The most commonly used objective approaches which include tests of outliers, data missing interpolation and homogeneity checks were employed to assess the quality of data (Feng et al., 2004; Wang et al., 2007; Klein Tank et al., 2009).

A second step was to assess homogeneity of data based on the penalized t-test (Wang et al., 2007) and the penalized maximal F-test (Wang, 2008). This stepwise testing algorithm is capable for detecting single or multiple changepoints in a time series based on a two-phase regression model (Wang, 2008). Monthly total rainfall and averaged temperature series were used to analyze homogeneity, based on the relative approach as described by Limsakul and Singhruck (2016). On the basis of the intensive quality control procedures, 41 and 40 high-quality records of rainfall and mean surface air temperature, respectively, for the period 1961 to 2016 was obtained (Figure 1) for further analysis.

As long-term records of digitized rice data are not available in Thailand, the annual rice production including area harvested and yield aggregated and/or averaged for whole Thailand during 1961-2016 were then extracted from the Food and Agriculture Organization Corporate Statistical Database (FAOSTAT) (FAO, 2018a). FAOSTAT is the world's most comprehensive database of food and agriculture statistics, with free access to national-level data for over 245 countries and territories from 1961 to the most recent year available. It is a major component of FAO's information system, contributing to multiple stakeholders use. The FAOSTAT database is used widely in peer-reviewed literature including many agriculture, forestry and other land use (AFOLU)-related analyses from global agriculture perspective studies (Foley et al., 2011) to land use change assessments and carbon cycle studies (Friedlingstein et al., 2011). Some of the FAOSTAT-derived indicators have been used to assess and measure progress towards the targets set in the 2030 Agenda for Sustainable Development, and to monitor national actions for climate change adaptation and mitigation in the context of Paris Agreement (FAO,

2018a). It typically receives around 200,000 visits per month from national statisticians, government officials, researchers, the private sectors, international agencies, civil society and the media from all over the world (FAO, 2018a).

In working directly with the member countries, typically via National Agriculture Statistical Offices, the Statistics Division of the FAO has been able to compile most of the official data and information. This process results in an internationally approved, coherent data platform covering key information for a large range of agriculture and forestry products worldwide (Tubiello et al., 2013; FAO, 2018a). FAO has been employing Statistics Quality Assurance Framework as a part of quality management system for statistics, and the structure for implementing quality assurance activities of the FAOSTAT (FAO, 2018a). Comparison of the rice production data extracted from FAOSTAT with the data obtained from Office of Agricultural Economics of Thailand for the short period of 2008-2016 shows that the values from both sources are almost the same.

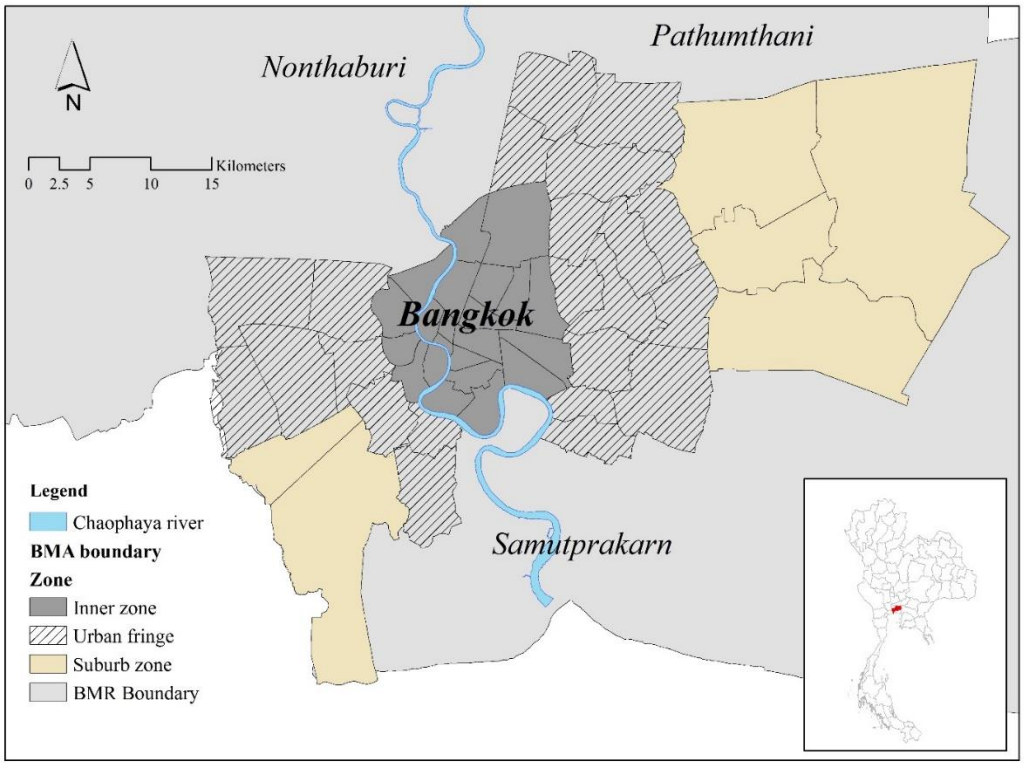


**Figure 1.** Location of the Bangkok Metropolitan Area

## 2.2 Image pre-processing

Time-series of LANDSAT 5 Thematic Mapper (TM) and LANDSAT 8 Thermal Infrared Sensor (TIRS) imageries (Path 129/Row 50, 51) acquired during 2008 and 2014 (LANDSAT 5 TM: 5 March 2008, 8 May 2008, 19 January 2009, 25 April 2009, 19 November 2009, 25 January 2011, 9 November 2011; LANDSAT 8 TIRS: 2 February 2014, 17 November 2014) were analyzed in this study. All of the images were clear and nearly cloud-free. Firstly, the radiometric and sun elevation correction was conducted. Next, the geometric correction was manipulated to be able to overlay and compare multi-temporal images or to interact with other mapping data. The LANDSAT images were rectified and georeferenced to the UTM map projection, datum WGS 84. Then, the images were resampled to 30 m using the nearest neighbor interpolation method to keep the brightness values of pixels unchanged. The root mean square (RMS) errors were less than 1 pixel.

## 2.3 Calculation of LST

In this study, the UHI of BMA is expressed with LST. The LST calculation methods are based on LANDSAT 5 and LANDSAT 8 User's Handbooks (NASA, 2011; USGS, 2019) which are widely used (Weng, 2009). To retrieve LST, the steps are as follows:

*2.3.1 Conversion of digital numbers to radiance*

First, the digital numbers (DN) of LANDSAT TM/TIRS thermal infrared bands were converted to radiance. For LANDSAT 5 TM thermal infrared band (band 6: 10.40-12.50 µm), the following equation (NASA, 2011) was used:

$$L_\lambda = ((L_{MAX} - L_{MIN}) / (QCAL_{MAX} - QCAL_{MIN})) \times (QCAL - QCAL_{MIN}) + L_{MIN} \quad (1)$$

Where, $L_\lambda$ is the spectral radiance at the sensor's aperture in W/($m^2$ster µm), $L_{MAX}$ and $L_{MIN}$ are the spectral radiance that is scaled to $QCAL_{MAX}$ and $QCAL_{MIN}$ in W/($m^2$ster µm), QCAL is the quantized calibrated pixel value in DN, $QCAL_{MAX}$(=255) and $QCAL_{MIN}$(=1) are the maximum and minimum quantized calibrated pixel value in DN.

For LANDSAT 8 TIRS thermal infrared bands (band 10: 10.60-11.19 and band 11: 11.50-12.51 µm), the radiance was calculated by using the following equation (USGS, 2019).

$$L_\lambda = M_L \text{ x } QCAL + A_L \quad (2)$$

Where, $L_\lambda$ is the top of atmosphere (TOA) spectral radiance in W/($m^2$srad µm), $M_L$ is the band-specific multiplicative rescaling factor from the metadata, $A_L$ is the band-specific additive rescaling factor from the metadata, QCAL is the quantized and calibrated standard product pixel values (DN).

*2.3.2 Conversion of digital numbers to radiance*

Next, the radiance obtained from Equations (1) and (2) was converted to brightness temperature by using the Equation (3) (NASA, 2011; USGS 2019).

$$T = K_2 / \ln [(K_1 / L_\lambda) + 1] \quad (3)$$

Where, T is the at-satellite brightness temperature in Kelvin (K), $K_2$ is the calibration constant 2=1282.71 K (in case of LANDSAT 5 TM) or band-specific thermal conversion constant from the metadata (K2_CONSTANT_BAND_x, where x is the band number, 10 or 11) (in case of LANDSAT 8 TIRS), $K_1$ is the Calibration constant 1=666.09 W/($m^2$ster µm) (in case of LANDSAT 5 TM) or band-specific thermal conversion constant from the metadata (K1_CONSTANT_BAND_x, where x is the band number, 10 or 11) (in case of LANDSAT 8 TIRS), $L_\lambda$ is the spectral radiance at the sensor's aperture in W/($m^2$ster µm) (in case of LANDSAT 5 TM) or top of atmosphere (TOA) spectral radiance in W/($m^2$srad µm).

Then, the brightness temperature was converted from Kelvin to Celsius (°C) by using the following equation. Finally, the surface radiance temperature maps of BMA at various times were manipulated.

$$T_S = T - 273.15 \quad (4)$$

Where, $T_S$ is surface radiance temperature in °C, T is at-satellite brightness temperature of a black body in K.

## 2.4 Analysis of LST variation and the UHII in BMA

To analyze the variation of surface temperature, the average surface temperature is calculated from the inner city, urban fringe, and suburb. Then, it is compared at each time period, such as monthly, seasonal and yearly. The intensity of urban heat island, UHII for the inner city, urban fringe, and suburb areas were determined by the following equations:

$$UHII_{(inner\text{-}suburb)} = \text{Surface temperature}_{inner} - \text{Surface temperature}_{suburb} \quad (5)$$

$$UHII_{(urban\ fringe\text{-}suburb)} = \text{Surface temperature}_{urban\ fringe} - \text{Surface temperature}_{suburb} \quad (6)$$

Then, the variation of surface temperatures and UHII in the inner city, urban fringe, and suburb areas were compared and described.

## 2.5 Analysis of UHII in BMA

*2.5.1 Analysis of relationship between UHII and NDVI*

First, the LANDSAT 5 band 3, 4 and LANDSAT 8 band 4, 5 were used to calculate the Normalized Difference Vegetation Index (NDVI) by using a following equation:

$$NDVI = (NIR - RED) / (NIR + RED) \quad (7)$$

Where, NDVI is the Normalized Difference Vegetation Index, NIR is the DN values from the near-infrared band, RED is the DN values from the red band.

Next, the proportion of vegetation covering the BMA were calculated by using the equation (Song et al., 2017) as shown:

$$F_r = (NDVI-NDVI0) / (NDVIs- NDVI0) \quad (8)$$

Where, $F_r$ is fractional vegetation cover, NDVI is Normalized Difference Vegetation Index, NDVI0 is bare soil NDVI, NDVIs is 100% vegetation cover.

Then, the relationship between surface temperature and vegetation coverage ($F_r$) was determined by using the regression model and confidence level from $R^2$.

*2.5.2 Analysis of relationship between UHII and high-rise buildings*

To analyze and describe the relationship between UHII and high-rise buildings in BMA, the cloud-free panchromatic GeoEye and WorldView-2 imageries, with resolution of 0.50 m, acquired during December-March of 2008 and 2014 were analyzed to classify the land use/land cover and height/density of buildings in the BMA area. Ground truth survey was conducted to validate and improve accuracy of the classified maps.

*2.5.3 Analysis of relationship between UHII and land use/land cover*

To analyze and describe the relationship between UHII and land use/land cover in BMA, the classified satellite imageries of BMA during 2008-2014 were used.

## 3. RESULTS AND DISCUSSION

### 3.1. Land surface temperature of BMA

The LANDSAT TM and TIRS thermal infrared bands worked very well to identify the LST of BMA (Figure 2).The highest temperature appeared in April 2009 at 41.07 ºC and the highest temperature during the month with the lowest minimum temperature occurred in November 2009 at 29.60 ºC in summer and winter, respectively, with a temperature difference of 11.47 ºC.

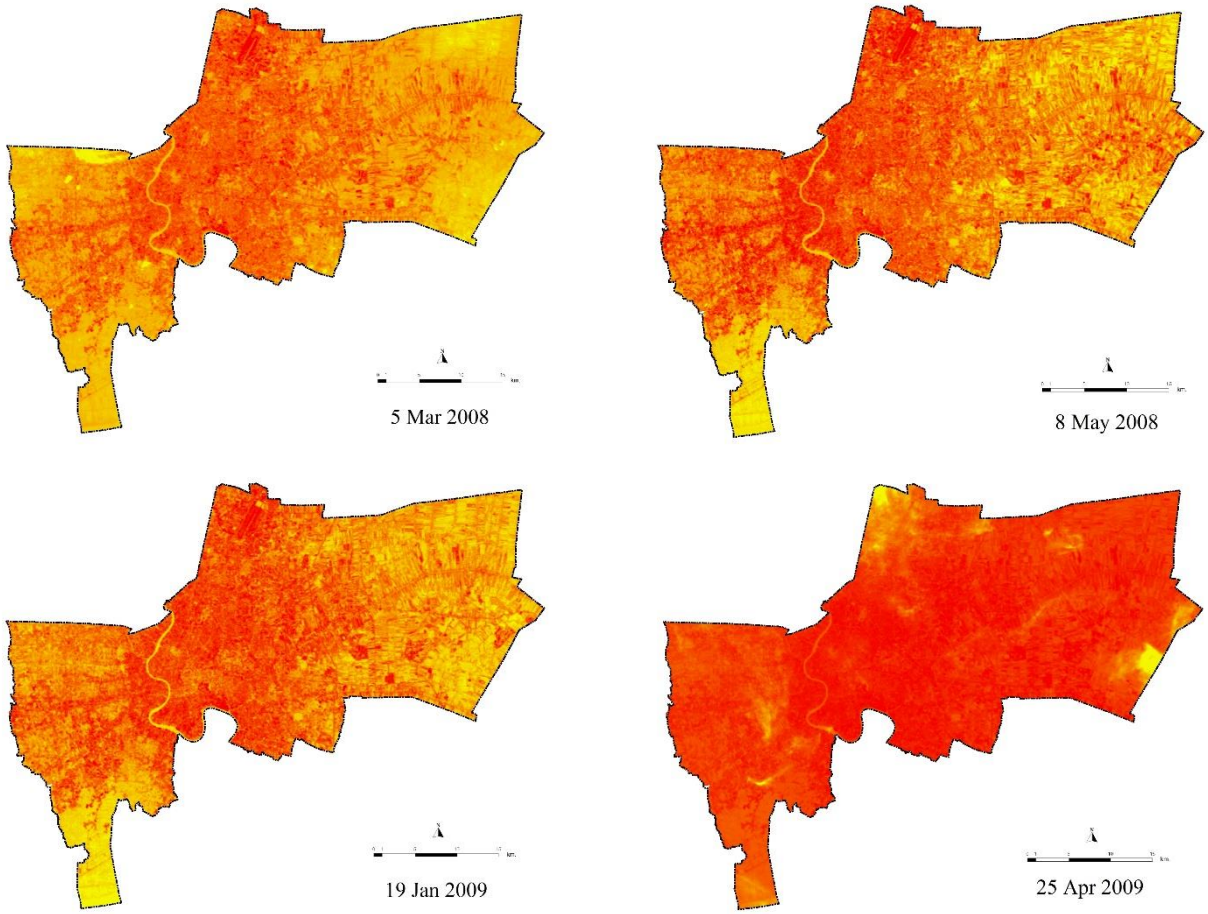


**Figure 2.** BMA land surface temperature map (ºC) in 2008, 2009, 2011 and 2014.

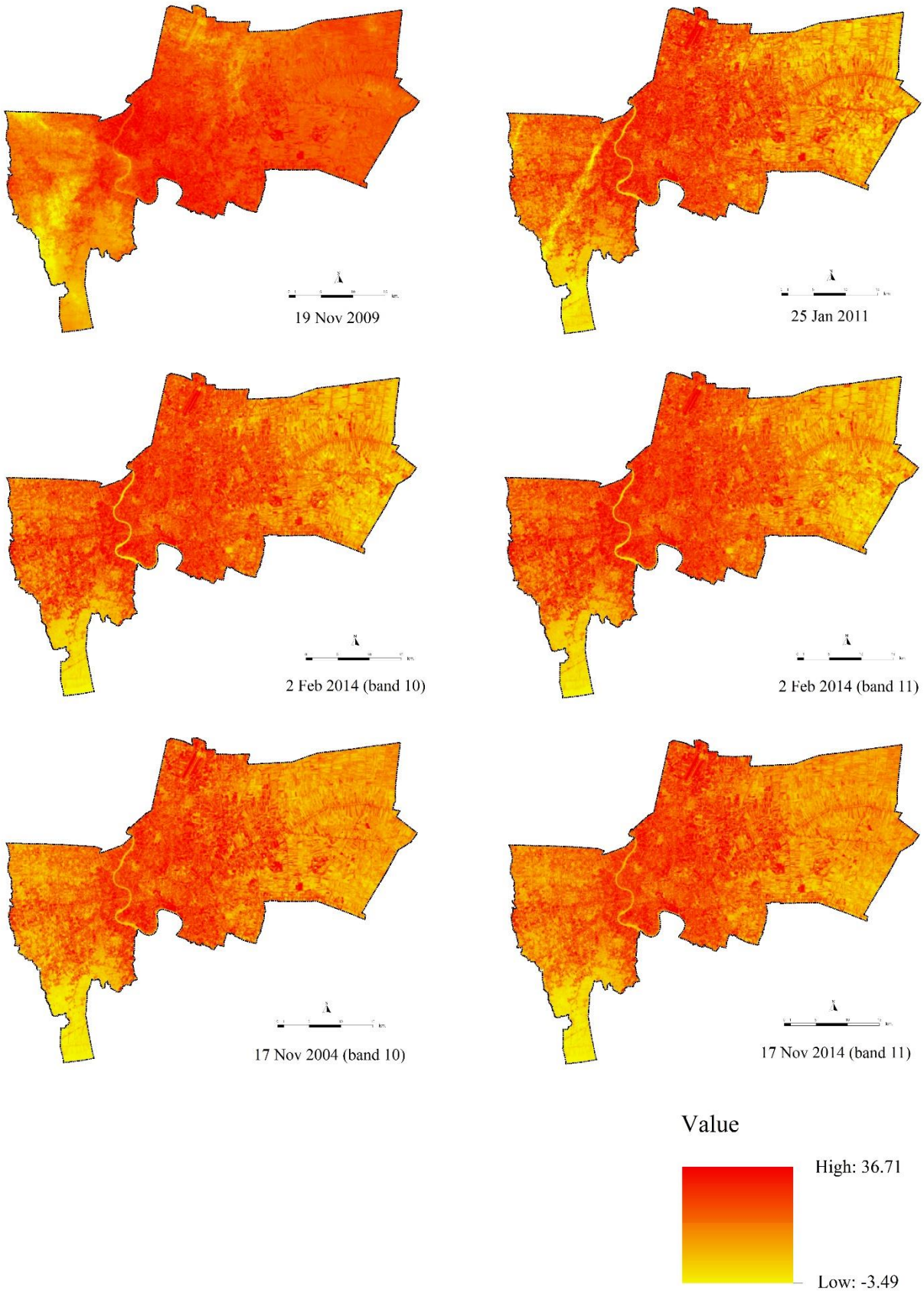


**Figure 2.** BMA land surface temperature map (°C) in 2008, 2009, 2011 and 2014 (cont.).

### 3.2 Surface temperature variation and the intensity of urban heat island in BMA

The results found that the average LST in the inner city (27.03 °C) is higher than the urban fringe (25.6 °C) and suburb area (23.96 °C). Also, the average LST in the urban fringe is higher than the average in the suburb area (Table 1 and Figure 3). In addition, the average surface temperature in the suburb area is different and the surface temperature variation from 2008 to 2014 is the highest, followed by the urban fringe and inner city area respectively.

For the BMA in total (Table 1), the average LST is in the range of 21-27 °C. By average, the maximum LST was in February 2014 (27.48 °C) and the average LST was lowest in November 2009 (21.97 °C) which is the winter season. It was also found that after 2011, the trend of average LST was higher. Especially in 2014, the average LST was higher than 27 °C.

**Table 1.** Average LST of 3 main areas (inner city, urban fringe, and suburb) and UHII in BMA (Unit °C).

| | Date | LST (°C) | | | | UHII | UHII |
|---|---|---|---|---|---|---|---|
| | | Inner city | Urban fringe | Suburb | BMA | (inner-suburb) | (urban fringe-suburb) |
| Summer | 5 Mar 2008 | 26.57 | 25.65 | 24.05 | 25.42 | 2.52 | 1.60 |
| | 8 May 2008 | 27.56 | 26.38 | 24.82 | 26.25 | 2.74 | 1.56 |
| | 25 Apr 2009 | 28.00 | 25.95 | 25.74 | 26.56 | 2.26 | 0.21 |
| | 2 Feb 2014 | 28.52 | 27.94 | 25.97 | 27.48 | 2.77 | 2.12 |
| | Average | | | | | 2.52 | 1.46 |
| Winter | 19 Jan 2009 | 26.14 | 25.32 | 23.54 | 25.00 | 2.60 | 1.78 |
| | 19 Nov 2009 | 23.86 | 21.26 | 20.79 | 21.97 | 3.07 | 0.47 |
| | 25 Jan 2011 | 27.39 | 26.59 | 24.72 | 26.23 | 2.67 | 0.95 |
| | 9 Nov 2011 | 27.16 | 23.99 | 20.24 | 23.80 | 6.92 | 3.75 |
| | 17 Nov 2014 | 28.09 | 27.34 | 25.80 | 27.08 | 2.58 | 1.72 |
| | Average | 27.03 | 25.60 | 23.56 | 25.53 | 3.31 | 1.67 |

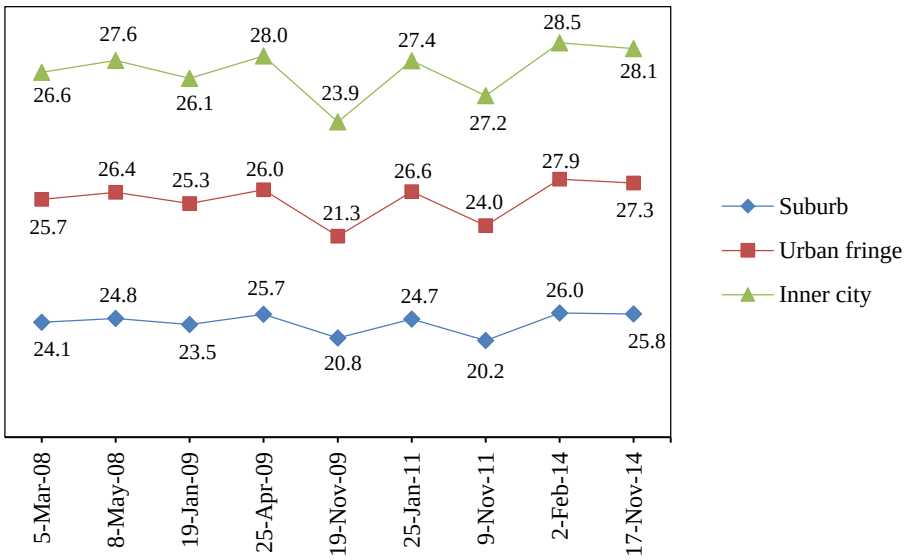


**Figure 3.** Comparison of Land surface temperature between inner, urban fringe and suburb in BMA

For urban heat island intensity (UHII), the UHII between inner city and urban fringe, and suburb were determined as shown in Table 1. In the summer of February 2014, the UHII between inner city and suburb areas was as high as 2.77 °C. The UHII between urban fringe and suburb areas was as high as 2.12 °C. In April 2009, there was a difference in the UHII between inner city and suburb of 2.26 °C with the UHII between urban fringe and suburb differing 0.21 °C.

Maximum UHII values were seen in November 2011, when the UHII between inner city and suburb areas was 6.92 °C and the UHII between urban fringe and suburb areas was 3.75 °C. It was found that the UHII between inner city and suburb areas was greater than the UHII between urban fringe and suburb areas.

The UHII from 2008 to 2014, shown in Table 1, indicates that in summer, the average UHII between inner city and suburb areas was 2.52 °C. The average UHII between urban fringe and suburb areas was 1.46 °C. In winter, the average UHII between inner city and suburb areas was 3.31 °C. The average UHII between urban fringe and suburb areas was 1.67 °C. The results of this study conclude that the average difference of the UHII between inner city and suburb areas and the average UHII between urban fringe and suburb area (1.06 °C) in summer is less than in winter. The average difference of the UHII between inner city and suburb areas with the average UHII between urban fringe and suburb areas was 1.64 °C. Therefore, the phenomenon of UHI in winter is higher than in summer in the Bangkok area.

### 3.3 Relationship between the UHII in BMA and various factors

*3.3.1 Relationship between the UHII in BMA and NDVI*

Figure 3 shows the NDVI of BMA in 2008, 2009, 2011 and 2014.It was found that the area with high NDVI will appear in urban fringe and suburb areas with plant cover and low LST. The area with low NDVI will appear in the inner city and urban fringe areas with construction area, open ground and high LST. When considering the difference in NDVI with inner city, urban fringe, and suburb areas, it was found that the inner city area in the year 2014 has an 83.33% lower NDVI than in 2008 It was also found that the urban fringe and suburb areas in 2014 have the NDVI lower by 71.43% than in 2008 (Table 2 and Figure 5). This is consistent with the results of Komonveeraket (1998).The study showed that the presence of vegetation could cool down the surface temperature in such land covers type. The decreasing of vegetation and the extension of built-up area can raise surface temperature.

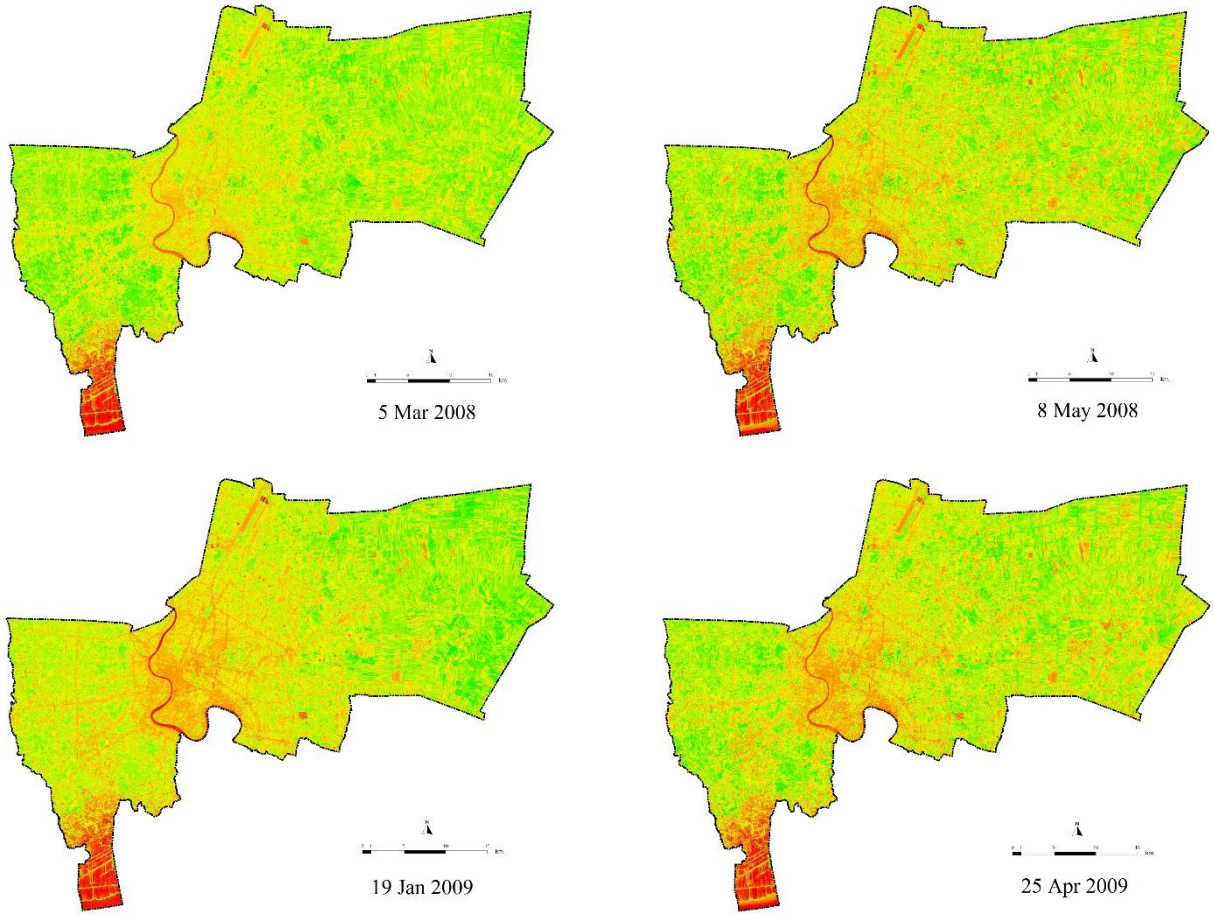


**Figure 4.** NDVI of BMA in 2008, 2009, 2011 and 2014.

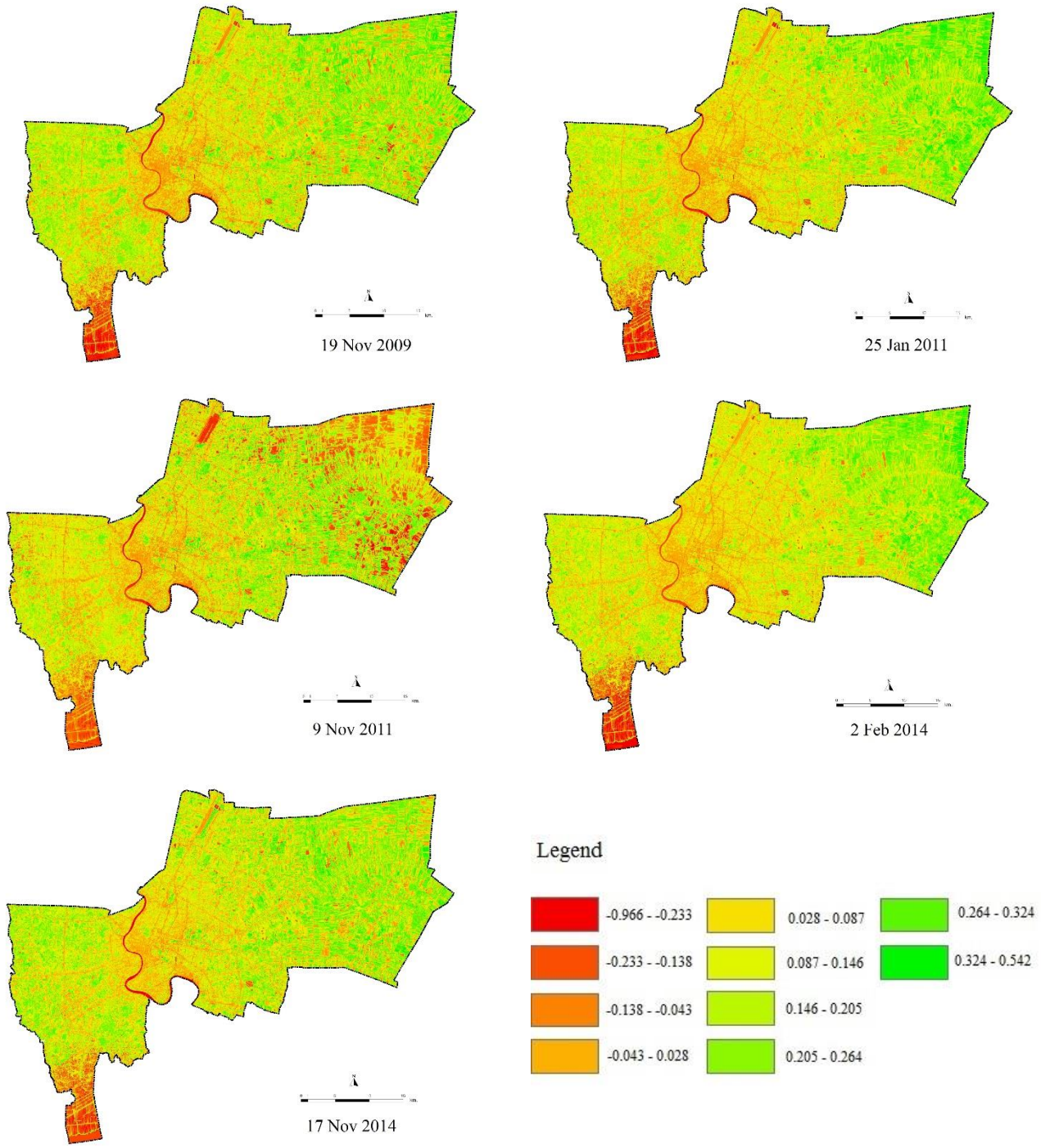


**Figure 4.** NDVI of BMA in 2008, 2009, 2011 and 2014 (cont.).

Considering the relationship between LST and vegetation coverage ($F_r$), it was found from regression equation model that the $F_r$ is negatively correlated with the surface temperature. In summer, the average confidence level ($R^2$) was 0.81. In winter, the average $R^2$ was 0.79 (Table 3 and Figure 6). When comparing the average $R^2$ for the relationship between the LST and $F_i$. It was found that the summer had a higher confidence level than the winter. This is consistent with the study of Li et al. (2012) and Meng and Liu (2013) which showed that significant LSTs gradients from the city center to surrounding rural areas reached a maximum during summer period.

**Table 2.** Average NDVI of the inner city, urban fringe, and suburb in 2008, 2009, 2011 and 2014.

| | Date | NDVI | | |
|---|---|---|---|---|
| | | Inner city | Urban fringe | Suburb |
| Summer | 5 Mar 2008 | 0.06 | 0.14 | 0.14 |
| | 8 May 2008 | 0.08 | 0.09 | 0.05 |
| | 25 Apr 2009 | 0.06 | 0.07 | 0.04 |
| | 2 Feb 2014 | 0.01 | 0.03 | 0.04 |
| Winter | 19 Jan 2009 | 0.03 | 0.06 | 0.04 |
| | 19 Nov 2009 | 0.07 | 0.09 | 0.05 |
| | 25 Jan 2011 | 0.05 | 0.08 | 0.06 |
| | 9 Nov 2011 | 0.01 | 0.07 | 0.03 |
| | 17 Nov2014 | 0.01 | 0.04 | 0.04 |

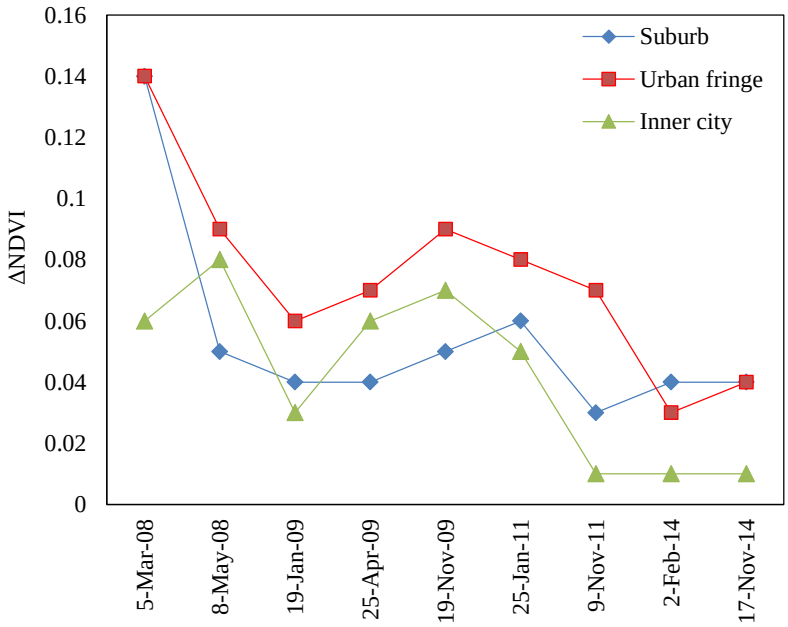


**Figure 5.** Comparison of NDVI of the inner, urban fringe, and suburb

**Table 3.** Relationship between LST and $F_r$.

| Season | Date | Fitted regression model | $R^2$ |
|---|---|---|---|
| Summer | 5 Mar 2008 | $LST = -8.462F_r + 27.23$ | 0.610 |
| | 8 May 2008 | $LST = -30.47F_r + 27.23$ | 0.923 |
| | 25 Apr 2009 | $LST = -43.74F_r + 29.89$ | 0.885 |
| | 2 Feb 2014 | $LST = -10.50F_r + 30.45$ | 0.821 |
| Winter | 19 Jan 2009 | $LST = -13.63F_r + 27.79$ | 0.778 |
| | 19 Nov 2009 | $LST = -19.29F_r + 23.70$ | 0.830 |
| | 25 Jan 2011 | $LST = -16.84F_r + 28.56$ | 0.869 |
| | 9 Nov 2011 | $LST = -25.49F_r + 25.55$ | 0.684 |
| | 17 Nov 2014 | $LST = -27.27F_r + 27.30$ | 0.787 |

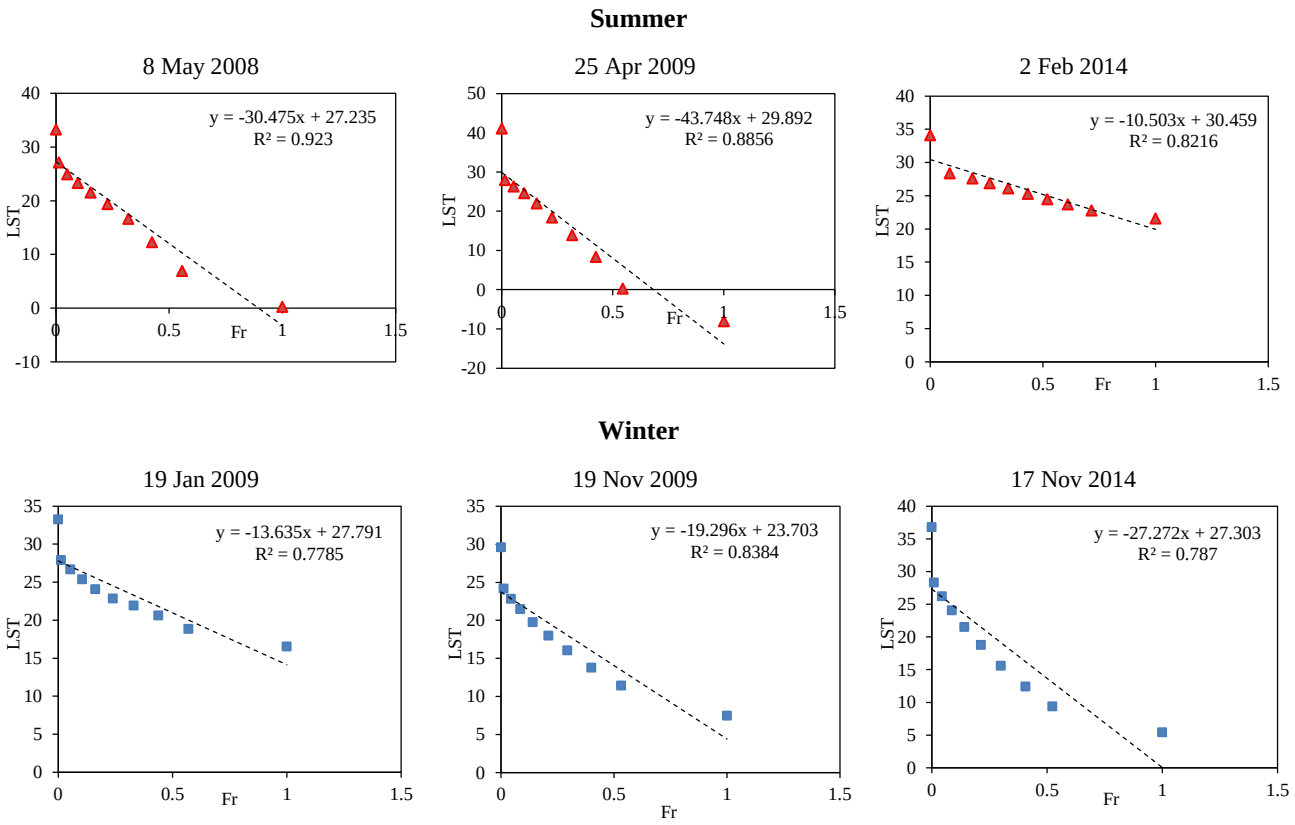


**Figure 6.** Relationship between LST and $F_r$.

*3.3.2 Relationship between the UHII in BMA and high-rise buildings*

From 2008 to 2014, there were about 500,000 new buildings in BMA. Also, Bangkok is experiencing rapid urban expansion. The urban growth rate during 2000-2009 was 2.41 % per year. The urban area in 2014 accounted for 56 % of the BMA. The buildings located in the inner city and urban fringe were a large high-rise building and increased the amount of vertical high density building. Figure 7 shows buildings in BMA in 2008, 2009, 2011 and 2014.

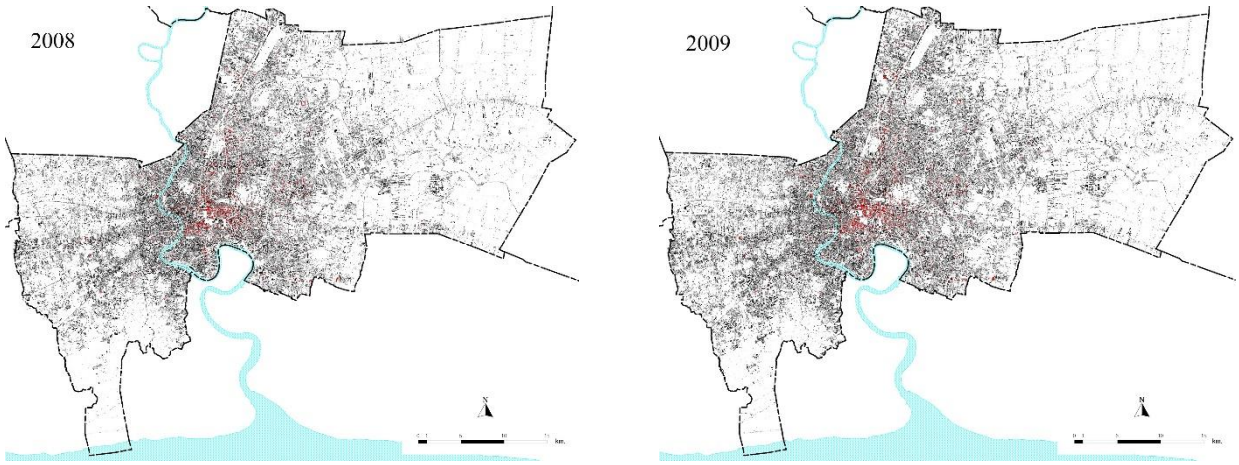


**Figure 7.** Buildings in BMA in 2008, 2009, 2011 and 2014

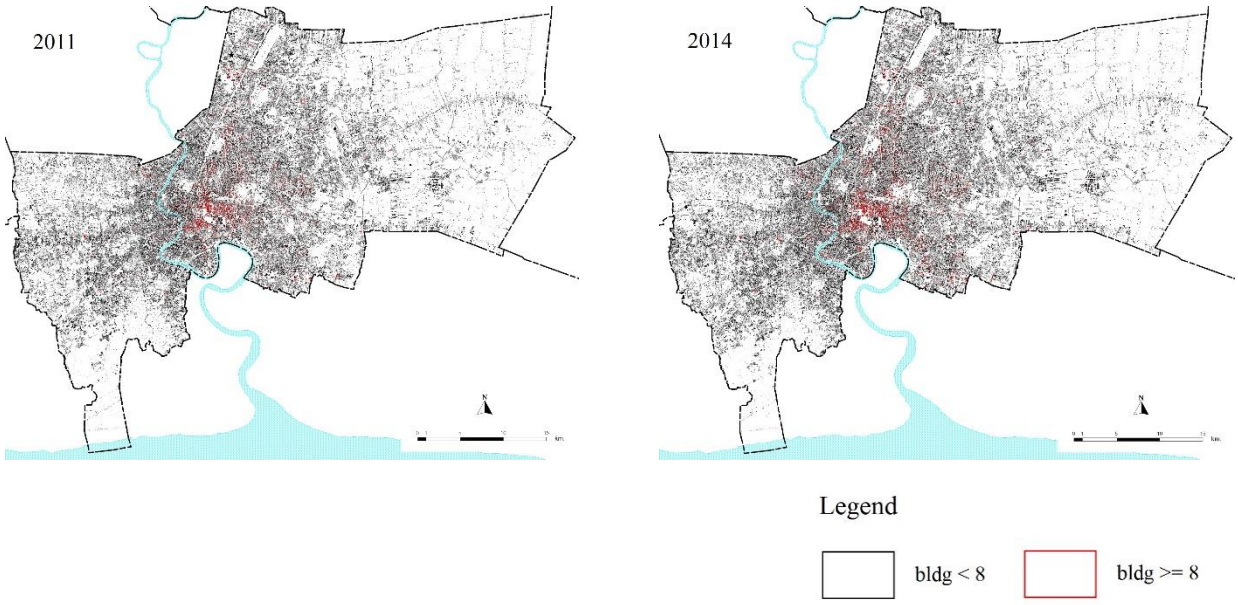


**Figure 7.** Buildings in BMA in 2008, 2009, 2011 and 2014 (cont.).

The number of high-rise buildings of 8 or more stories in inner city and urban fringe areas of BMA from 2008 to 2014 increased. Due to limited city space, the buildings have increased vertically, especially in the inner city. In 2008, 2009, 2011, and 2014, there were 2,452, 3,072, 3,096, and 4,603 high-rise buildings, respectively. The high-rise buildings in inner city areas increased by 2,151 units between 2008 and 2014, whereas in the urban fringe and suburb areas they increased by 1,432 and 101 units, respectively.

The increase in the number of high-rise buildings and higher building density affects LST and caused UHI phenomena in the city. Hence, the UHII between inner city and suburb areas of BMA was higher than the UHII between urban fringe and suburb areas in summer and winter. Most of the concrete was used for buildings and constructions. It affected the reflection and absorbed energy from the sun. The increase in buildings and structures occurred and absorbed more energy from the sun than the ground and vegetation, making the surface temperature of the buildings higher. The heat that has been stored in building materials and buildings will reflect back into the atmosphere and increase the air temperature in urban areas. The result of UHI phenomenon in the city is more heat. This corresponds to the cause of the UHI phenomenon (U.S. EPA, 2014). This agrees with Poolakhon and Boonyaputthipong (2013) where the increment of surface temperature responsible by existing of concrete and asphalt materials was reported.

*3.3.3 Relationship between the UHII in BMA and land use/land cover*

According to the land use/land cover maps of BMA in 2008, 2009, 2011 and 2014 (Figure 8), the inner city area of BMA contains a high-density of commercial and residential land use. Government agencies and educational institutions were scattered in the BMA. The urban fringe area is an area that supports the fragmentation of the city, the density of residential land use, and the distribution of commercial land use in industry. South of the BMA is the area of Bangna and Prawet. Agricultural land use is in the west. The unused land is spread on the east side of the BMA for development to accommodate the expansion of the city. The land use of the suburb area is mostly agricultural. The land west of the suburb area in Bang Khun Thian is used for industry.

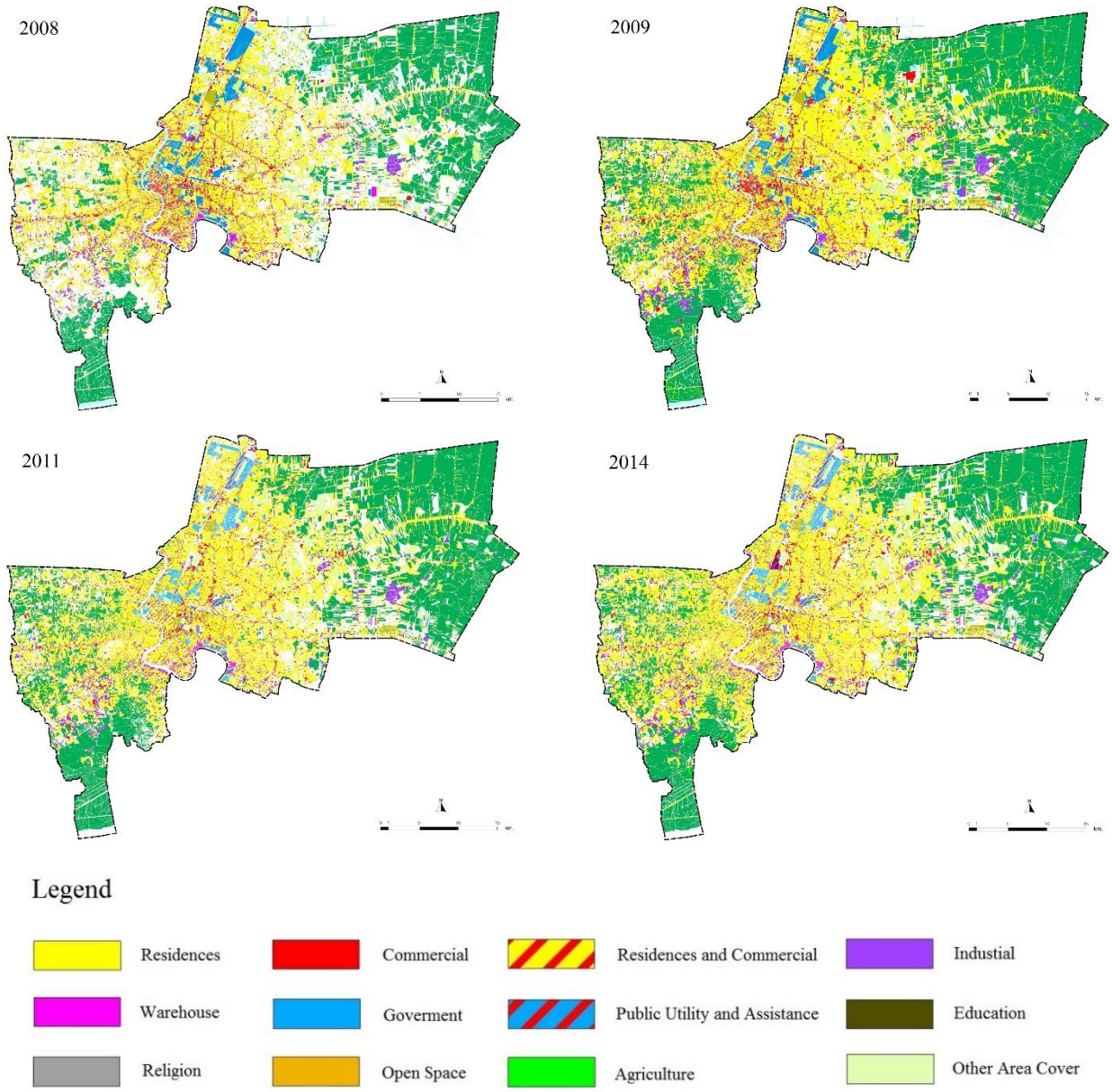


**Figure 8.** Land use/land cover maps of BMA in 2008, 2009, 2011 and 2014.

**Table 4.** Land use data of BMA in 2008, 2009, 2011 and 2014 (in $km^2$) by 3 main areas.

| Zone | Land use | 2008 | 2009 | 2011 | 2014 |
|---|---|---|---|---|---|
| Inner city | Urban/Built-up | 221.39 | 222.48 | 225.28 | 226.07 |
| | Agriculture | 2.58 | 2.24 | 2.41 | 2.06 |
| | Open Space | 3.92 | 2.65 | 4.00 | 4.87 |
| | Others | 31.97 | 32.31 | 16.85 | 14.32 |
| Urban fringe | Urban/Built-up | 343.81 | 364.17 | 387.63 | 422.53 |
| | Agriculture | 85.61 | 85.13 | 84.17 | 83.14 |
| | Open Space | 8.79 | 6.76 | 9.32 | 9.15 |
| | Others | 150.44 | 141.57 | 125.66 | 105.22 |
| Suburb | Urban/Built-up | 159.06 | 178.90 | 206.10 | 229.72 |
| | Agriculture | 415.15 | 395.76 | 377.03 | 367.47 |
| | Open Space | 3.57 | 3.48 | 5.89 | 5.74 |
| | Others | 142.43 | 133.10 | 124.39 | 97.64 |
| | Total | 1,568.73 | 1,568.73 | 1,568.73 | 1,568.73 |

From Table 4, the urban/built-up area has increased by 21.27% (from 724.26 $km^2$ in 2008 to 878.32 $km^2$ in 2014). The increase in urban/built-up area was 154.06 $km^2$ between 2008 and 2014 when compared to the agricultural area. In contrast, during 2008-2014, the agricultural area was decreased by 50.67 $km^2$. The open area was increased to 3.47 $km^2$and the area covered by other types was decreased to 106.86 $km^2$. In summary, the urban/built-up area, and open space were increased by 21.27% and 21.32%, while agricultural area, and area covered by other types, were decreased by 10.06% and 32.89%, respectively. It seems that the annual rate of urbanization was slower between 2011 and 2014 (0.12% yearly) compared to the 2009-2011 period (0.63%). The increase and expansion of cities or buildings will result in the decrease of agricultural and other covered areas, which will affect LST and UHI phenomena.

Comparing with the intensity of urban heat island, it was found that land use changes, agricultural areas and other vegetation covered areas were replaced by more cities and buildings. In 2014, when there were more urban areas and buildings in the inner city, urban fringe, and suburb areas the UHII between inner city and suburb areas was (2.77 °C) in the summer and the UHII between the urban fringe and suburb areas was the highest (2.12 °C). The highest UHII measured was in the winter of 2011, when the UHII between inner city and suburb areas was 6.92 °C and the UHII between urban fringe and suburb areas was 3.75 °C.

The trees and vegetation provide shade, which reduces the surface temperature. In urban area, the processes of evaporation of plant water, and evaporation of water from the ground were less. As a result, the surface temperature and air temperature in urban areas were increased. This corresponds to the cause of urban heat island phenomenon (U.S. EPA, 2014). It was also found that the surface temperature was high in inner city areas with high density of cities and buildings, and low in agricultural and open spaces. The areas with the lowest surface temperature was the suburb area followed by the urban fringe, respectively correlating with their low density of cities and buildings, and high density of agricultural and open space. This is in line with the results of Teanmanee (2002) and Komonveeraket (1998) that indicated the high temperature and UHI phenomena appeared on highly dense areas with complex constructions and human activities.

## 4. CONCLUSIONS

In this research, time-series LANDSAT thermal infrared bands have been used to study the variation of LST and the UHII phenomenon in BMA. Between 2008 and 2014, the highest LST was in the summer and the lowest LST was in the winter. It was found that the trend of UHII between inner city and suburb areas was higher than UHII between urban fringe and suburb areas. The average UHII between inner city, urban fringe, and suburb areas in winter is 1.64 °C which is higher than the corresponding average UHII of 1.06 °C. Therefore, the phenomenon of UHI in BMA in winter is higher than in summer. The UHI phenomena are linked to higher LST. The factors that affected the UHI phenomenon in this research are the NDVI, high-rise buildings, and land use/land cover. It was found that the LST correlated inversely with the NDVI. If the LST is high, the NDVI value is low in the city or building areas. Urban areas have low amounts of open space, agricultural and other vegetation covered areas. The high buildings and very high building density in inner city and urban fringe areas affects the reflection and absorption of energy from the sun. For the low LST, the NDVI value is high in agricultural land and other vegetation covered areas that have low density buildings such as in outer city or suburb areas.

Based on this research, a guideline for reducing the UHII phenomena in inner city, urban fringe, and suburb areas of BMA is to add a green space. However, space is limited in the inner city which has tall and very dense buildings for commercial and residential use. There is less open space and green space. One way to increase green areas is by building vertical gardens, green roofs and cool roofs for greener city strategy. For example, it can have gardening along a fence or a long wall or garden roof to reduce the temperature of the city and reduce the absorption of heat from the sun by the building. BMA should consider contributions of green space to urban cooling in all urban development and encourage developers to integrate green spaces such as rooftop gardens with their high-rise building projects. This study investigated only the factors of the NDVI, high-rise buildings, and land use in BMA. Other factors should be studied, such as air temperature, wind speed

and direction, and the use of data from more air monitoring stations in microclimate. These factors may affect the phenomenon of UHI in BMA as well.

## ACKNOWLEDGEMENTS

The authors would like to thank Bangkok Metropolitan Administration for their support. Also, thank you to the other agencies that support the information in the research. Authors wish to thank Thomas Neal Stewart, Mahidol University for improvement of the manuscript.

## REFERENCES

Balçik BF. Determining the impact of urban components on land surface temperature of Istanbul by using remote sensing indices. Environmental Monitoring and Assessment 2014;186:859-72.

Bangkok Information Center. Bangkok Nowadays [Internet]. 2015. Available from: http://www.bangkokgis.com/gis_information/population/ (in Thai).

Chayapong P. Spatial Analysis of Urban Heat Island Phenomenon and Its Relationship with Land Use and Land Cover and Electrical Energy Consumption: A Case Study in Bangkok Metropolitan Area [dissertation]. Nakhon Ratchasima, Suranaree University of Technology; 2010.

Chen XL, Zhao HM, Li PX, Yin ZY. Remote sensing image-based analysis of the relationship between urban heat island and land use/cover changes. Remote Sensing of Environment 2006;104:133-46.

Department of City Planning. Final Report of the Project on BMA Central City Planning (3rd Revision). Bangkok, Department of City Planning BMA; 2011 (in Thai).

Grimm NB, Faeth SH, Golubiewski NE, Redman CL, Wu J, Bai X, Briggs JM. Global change and the ecology of cities. Science 2008;319:756-60.

Hung T, Uchihama D, Ochi S, Yasuoka Y. Assessment with satellite data of the urban heat island effects in Asian mega cities. International Journal of Applied Earth Observation and Geoinformation 2006;8:34-48.

Imhoff ML, Zhang P, Wolfe RE, Bounoua L. Remote sensing of the urban heat island effect across biomes in the continental USA. Remote Sensing Environment 2010;114:504-13.

Jiang XD, Xia BC, Guo L. Research on urban heat island and its environmental effects of rapidly urbanized regions. Ecologic Science 2006;25:171-5.

Keramitsoglou I, Kiranoudis CT, Ceriola, G, Weng Q, Rajasekar U. Identification and analysis of urban surface temperature patterns in Greater Athens, Greece, using MODIS imagery. Remote Sensing of Environment 2011;115:3080-90.

Komonveeraket K. The Effects of Land Cover on Urban Heat Islands in Bangkok Metropolis [dissertation]. Bangkok, Chulalongkorn University; 1998 (in Thai).

Li YY, Zhang H, Kainz W. Monitoring patterns of urban heat islands of the fast-growing Shanghai metropolis, China: Using time-series of LANDSAT TM/ETM+ data. International Journal of Applied Earth Observation and Geoinformation 2012;19:127-38.

Lo CP, Quattrochi DA, Luvall JC. Application of high-resolution thermal infrared remote sensing and GIS to assess the urban heat island effect. International Journal of Remote Sensing 1997;18:287-304.

Manjula R, Ronal CE, Yuji M. An urban heat island study of the Colombo Metropolitan Area, Sir Lanka, based on LANDSAT data(1997-2017). ISPRS International Journal of Geo-Information 2017;6:189.

Meng F, Liu M. Remote-sensing image-based analysis of the patterns of urban heat islands in rapidly urbanizing Jinan, China. International Journal of Remote Sensing 2013;34(24):8838-53.

National Aeronautics and Space Administration (NASA). Landsat 7 Science Data Users Handbook. Washington D.C., USA: National Aeronautics and Space Administration; 2014.

Nichol JE. High-resolution surface temperature patterns related to urban morphology in a tropical city: asatellite-based study. Journal of Applied Meteorology and Climatology 1996;35:135-46.

Pongrácz R, Bartholy J, Dezsö Z. Application of remotely sensed thermal information to urban climatology of central European cities. Physics and Chemistry of the Earth 2010;35:95-9.

Poolakhon B, Boonyaputthipong C. The comparing of Heat on concrete and asphalt. Proceedings of the 9th Mahasarakham Research Conference; 2013 September 12-13; Bangkok; 2014.

Qin Z, Karnieli A, Berliner P. A Mono-window algorithm for retrieving land surface temperature from LANDSAT TM data and its application to the Israel-Egypt border region. International Journal of Remote Sensing 2001;22:3719-46.

Song W, Mu X, Ruan G, Gao Z, Li L, Yan G. Estimating fractional vegetation cover and the vegetation index of bare soil and highly dense vegetation with a physically based method. International Journal of Applied Earth Observation and Geoinformation 2017;58:168-76.

Streutker DR. A remote sensing study of the urban heat island of Houston, Texas. International Journal of Remote Sensing 2002;23(12):2595-608.

Streutker DR. Satellite-measured growth of the urban heat island of Houston, Texas. Remote Sensing of Environment 2003;85:282-9.

Teanmanee T. Urban heat island and urban physical environment [dissertation]. Nakhon Pathom, Silpakorn

University; 2002 (in Thai).

Tongliga B, Xueming L, Jing Z, Yingjia Z, Shenzhen T. Assessing the distribution of urban green spaces and its Anisotropic cooling distance on urban heat island pattern in Baotou, China. ISPRS International Journal of Geo-Information 2016;5(2):12.

United States Environmental Protection Agency (U.S. EPA) Reducing Urban Heat Islands: Compendium of Strategies: Chapter 1: Urban Heat Island Basics. USA: United States Environmental Protection Agency; 2012.

U.S. Geological Survey (USGS). Landsat 8 Data Users Handbook. USA: US Geological Survey; 2019.

Voogt JA, Oke TR. Thermal remote sensing of urban climates. Remote Sensing of Environment 2003;86: 370-84.

Weng Q. Thermal infrared remote sensing for urban climate and environmental studies: methods, applications, and trends. ISPRS Journal of Photo-grammetry and Remote Sensing 2009;64:335-44.

Weng Q, Fu P, Gao F. Generating daily land surface temperature at LANDSAT resolution by fusing LANDSAT and MODIS data. Remote Sensing of Environment 2014;145:55-67.

Weng Q, Liu H, Lu D. Assessing the effects of land use and land cover patterns on thermal conditions using landscape metrics in city of Indianapolis, United States. Urban Ecosystems 2007;10(2):203-19.

Weng Q, Lu D, Schubring J. Estimation of land surface temperature-vegetation abundance relationship for urban heat island studies. Remote Sensing of Environment 2004;89(4):467-83.

Xu HQ, Chen BQ. Remote sensing of the urban heat island and its changes in Xiamen City of SE China. Journal of Environmental Sciences 2004;16:276-81.

Yuan F, Bauer ME. Comparison of impervious surface area and normalized difference vegetation index as indicators of surface urban heat island effects in LANDSAT imagery. Remote Sensing of Environment 2007;106(13):375-86.

Zhang L, Meng Q, Sun A, Sun Y. Spatial and temporal analysis of the mitigating effects of industrial relocation on the surface urban heat island over China. ISPRS International Journal of Geo-Information 2017;6(4): 121.

Zhou D, Zhao S, Liu S, Zhang L, Zhu C. Surface urban heat island in China's 32 major cities: spatial patterns and drivers. Remote Sensing of Environment 2014;152:51-61.